New Research Progress in Ti_2AlCN MAX Phases and Their Reinforced Magnesium Composites

New Research Progress in Ti_2AlCN MAX Phases and Their Reinforced Magnesium Composites

By

Wenbo Yu

Cambridge Scholars Publishing

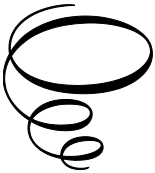

New Research Progress in Ti_2AlCN MAX Phases and Their Reinforced Magnesium Composites

By Wenbo Yu

This book first published 2022

Cambridge Scholars Publishing

Lady Stephenson Library, Newcastle upon Tyne, NE6 2PA, UK

British Library Cataloguing in Publication Data
A catalogue record for this book is available from the British Library

ISBN (10): 1-5275-8318-X
ISBN (13): 978-1-5275-8318-4

The people who get on in this world are the people who get up and look for circumstances they want, and if they cannot find them, make them.

——Bernard Shaw

CONTENTS

PREFACE

$M_{n+1}AX_n$ phases (M: transition metal, A: IIIA or IVA group element, and X: either carbon or nitrogen) are a class of ternary nitrides and carbides (n = 1 to 3), which possess both metal and ceramic-like properties. While they show the machinability, thermal shock resistance and electrical and thermal conductivity of metals, their high stiffness and corrosion and oxidation resistances are similar to those of ceramics. Up to now, more than 70 MAX phases have been synthesized. These phases have a hexagonal crystal structure that consists of edge-sharing $[M_6X]$ octahedrons interleaved with A layers; they are thus considered nanolaminated-layered materials. Strong M-X bonds and weaker M-A bonds associated with the nanolayered nature of the structure endow these solids with their unique combination of metal and ceramic properties. Furthermore, MAX phase solid solutions can be formed on any of the three sub-lattices: the M, A and X sites. This extra degree of freedom implies that the chemical/physical properties of the MAX phases may be modified and optimized by the replacement of various elements in the structure. Hence, MAX phases and MAX phase solid solutions have aroused great interest among scientists in physics, chemistry, and materials science.

Even if the stoichiometry of the $M_{n+1}AX_n$ compounds is generally assumed to be 2:1:1; 3:1:2 and 4:1:3 for n = 1, 2 or 3 respectively, differences from this "ideal" stoichiometry can exist and can strongly influence the physical properties. In other words, it would be of interest to know, not only the microstructure, but also the exact stoichiometry of the MAX phase compounds when comparing properties of MAX phases samples. As a result, one can think that the physical and chemical properties of MAX phases may be tuned by playing with substitution and vacancy content.

$Ti_2Al(C_xN_{1-x})$ compounds are one of the most important examples of MAX phase solid solutions on the X site. Since Ti-N and Ti-C have similar chemical bonding characteristics, resembling those of binaries TiC and TiN compounds, it is thus possible to form a wide range of $Ti_2Al(C_xN_{1-x})$ solid solutions with different physical properties. Indeed, the titanium-based compounds have been intensively investigated for high-temperature ohmic contacts on wide gap semiconductors. As a prerequisite

to their application for electrical contacts, the electronic properties of MAX phases, especially their anisotropic transport properties, and their modifications resulting from solid solution and/or vacancy effects have to be properly studied and understood.

Although intensively studied, the anisotropy of the MAX phase transport properties remains a complex issue since the majority of transport experiments were performed on polycrystalline samples, thereby averaging the basal plane and c-axis transport properties. To circumvent this point, several alternative approaches have been investigated, such as the probe of single grain plasmon excitation using electron energy-loss spectroscopy (EELS), the comparison between data obtained on (000l)-oriented thin films and bulk polycrystalline samples, or the comparison between thin films with different grain populations. In the two latter cases, the conductivity anisotropy is evidenced since the (000l)-oriented thin film room temperature (RT) resistivity and electron-phonon interactions are different from either the data recorded on the polycrystalline sample or the thin film exhibiting a different grain population.

In applications where high-temperature oxidation resistance in air is required, the oxidation kinetics of Ti_2AlC and Ti_3AlC_2 have been investigated. Their weight gain vs. time data is documented by cubic and parabolic models in air in the range of 800 to 1300 °C, as presented. Until now, there have been few reports to clarify these two mechanisms.

As a response to the increasing demand for new materials, tailored property composites are highly promising. One example is a composite of copper and MAX phases. In the framework of MAX-Cu composites, Ti-based MAX phases including Ti_3AlC_2, Ti_2AlC and Ti_2AlN have been used. It was reported that the de-intercalation of Al along basal planes induces the formation of Ti_xC platelets in Ti_3AlC_2-reinforced Cu composites. However, a comprehensively atomic-scale evolution during the diffusion of Cu in the Ti_2AlC MAX phase has not been investigated.

Among all structural materials, Mg alloys are regarded as the most attractive candidates for the reduction of vehicle weights, owing to their low density. However, the disadvantages of their poor stiffness and elevated temperature tensile strength restrict their wide utilization for applications. Hence, the development of new magnesium-based materials such as magnesium-based composites combining good mechanical properties, excellent tribological performance and a high damping capacity has become a hot research topic in recent years.

In such a context, this book is divided into seven chapters. Chapter 1 is a general introduction of MAX phases. It also describes lattice and electronic structures of the main MAX phases, and experimental and

theoretical research work on synthesis, mechanical and transport properties of the Ti-Al-C-N system. In addition, the vacancy effect and anisotropic transport properties of MAX phases are described.

Chapter 2 is devoted to the synthesis and microstructural characterization of highly pure and dense stoichiometric and substoichiometric $Ti_2Al(C_xN_y)$ solid solutions and related Ti_2AlC_x and Ti_2AlN_y end-members.

Chapter 3 deals with the mechanical and transport properties with respect to the vacancy content and solid solution effects in the Ti-Al-C-N system.

Chapter 4 is devoted to the anisotropic transport properties of Ti_2AlC and Ti_3SiC_2. Chapter 5 is about the grain size effect in the oxidation behavior of Ti_2AlC and the atomic level reaction behavior between Ti_2AlC and Cu.

Chapter 6 and Chapter 7 deal with the mechanical properties, damping behavior and tribological properties of Mg composites reinforced by Ti_2AlC and Ti_3SiC_2 MAX phases. Some of the potential applications for these composites are introduced.

As is always the case, there have been many people who have influenced the work concerned in this thesis. I am especially, deeply grateful to my Ph.D. supervisors, Sylvain Dubois and Véronique Gauthier-Brunet, and my master's supervisor, Shibo Li. It is certainly through their guidance, understanding, patience, and encouragement that I started to work on Ti_2AlCN. With their guidance, I grow not only as an experimentalist but also as an instructor and an independent thinker. I would like to give my thanks to Profs. Thierry Cabioc'h and Vincent Mauchamp. Thanks for use of the Rietveld refinement and theoretical explanation by ab initio calculations. Thanks to Prof Shoumei Xiong I had the inspiration for the introduction of MAX phases into a Mg matrix and fortunately was financed by the National Science Foundation of China and the State Key Lab of Advanced Metals and Materials.

I am also delighted to work with my collaborators Maxime Vallet, Antoine Guitton, Julien Guénolé and Weiwei Sun who made an everlasting impression on me with their talents and personalities. In addition, I am deeply appreciative of my student Chaosheng Ma due to his effortless corrections of the format of this manuscript.

Moreover, I am heartily thankful to Yang Zhou, Cuiwei Li and Zhengying Huang for their infinite help, not only with scientific problems, but also with personal ones. It is always wonderful to pass agreeable moments with them in the same office.

Last but not least, I am grateful for the support of the National Natural Science Foundation of China (No. 52175284 and 51701010), the State

Key Lab of Advanced Metals and Materials (No. 2021-ZD08), and the Pre-Research Program in National 14 th Five-Year Plan (No. 80923010304).

CHAPTER 1

INTRODUCTION

1.1. Introduction of MAX phases

1.1.1. History, definition and interest

In the 1960s, Hans Nowotny's group in Vienna discovered more than 100 new carbides and nitrides, accomplishing a gargantuan body of work[1]. Among these carbide and nitride phases were the so-called "Hägg phases" or "H phases" and their relatives Ti_3SiC_2 and Ti_3GeC_2. H phases are constituted of M_2X units (where M is a transition metal, and X is C and/or N) separated by the pure planes of an A-element (A being mostly an element of column IIIA or IVA of the periodic table); their chemical formula is M_2AX. The structures of Ti_3SiC_2 and Ti_3GeC_2 are similar to those of H phases—consisting of alternating pure Si or Ge planes and Ti_3C_2 units[1]. In the 1970s, a Russian group published work on the synthesis of Ti_2AlN and Ti_2AlC phases[2, 3], however, this work is unrecognized. This Russian group announced that the micro-hardness of these materials is in the range 21-24 GPa [2, 3], which is not compatible with the values admitted recently (3-12 GPa, see Table 1-7)[4]. Despite the impressive accomplishment of Novotny's group, these phases remained largely unexplored until the 1990s, when several researchers began to take a renewed interest in the H phases. The breakthrough contribution that triggered a renaissance came in the mid-1990s, when M. W. Barsoum and T. El-Raghy synthesized relatively pure-phase samples of Ti_3SiC_2[5] and revealed a material with a unique combination of metallic and ceramic properties. Like metals, Ti_3SiC_2 exhibits high electrical and thermal conductivities, and it is machinable. Moreover, it appears, like ceramics, to be extremely resistant to oxidation and thermal shock. Barsoum et al. demonstrated that Ti_3SiC_2 has a high yield point and presents plasticity behavior at 1300 °C. Furthermore, it is a self-lubricant. When M. W. Barsoum et al. later discovered Ti_4AlN_3[6], it became clear that these phases share a basic structure that gives them similar properties. This achievement led to the introduction of the "$M_{n+1}AX_n$ phases" (n = 1, 2, or

3) or “MAX phases” nomenclature, where M is a transition metal, A is an A-group element, and X is C and/or N (see Fig. 1-1).[7]

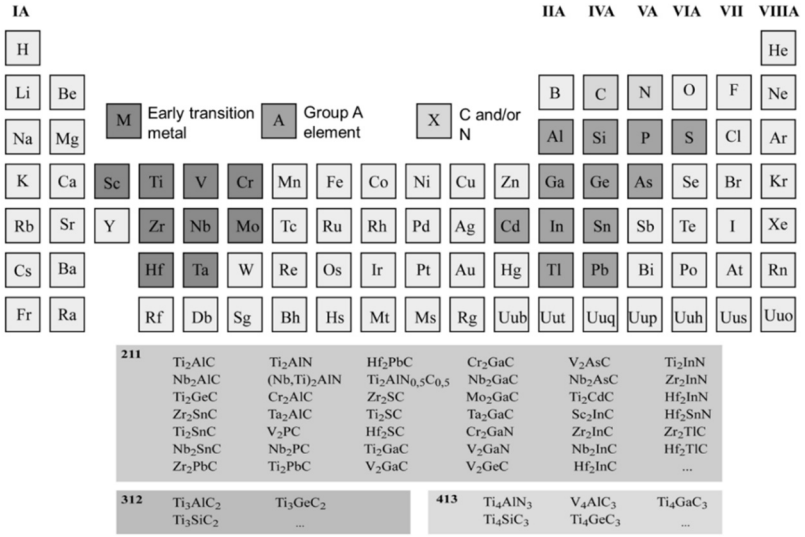

Fig. 1-1: Location of the elements of $M_{n+1}AX_n$ ternary nitrides and carbides in the periodic table[7].

From their lamellar structure, MAX phases are characterized by the exceptionally robust M-X bonds interleaved with the relatively weak M-A bonds. Therefore, MAX phases exhibit a combination of the merits of both metals and ceramics. Like ceramics, they are resistant to chemical attack, are oxidation resistant, quite stiff, and have relatively low thermal expansion coefficients[4, 8, 9]. Like metals, they are resistant to thermal shock, thermally and electrically conductive, damage tolerant and deform plastically at elevated temperatures[4, 8, 9]. Plastic deformation occurs via kink and shear band formation (see Fig. 1-2)[10-12]. Kink bands show almost no cracks at their boundaries (Fig. 1-2a) and the kink bands in $Cr_2Al(Si)C$ can even bend to 180° without fracture[13]. In the hexagonal structure of the MAX phases, dislocation slip is supposed to occur only in the basal planes. As dislocations are thought to be confined to basal planes[10, 14], they arrange themselves either in arrays in the basal plane or in walls perpendicular to basal planes [10]. Two dislocation walls of opposite Burgers vector form a kink band.

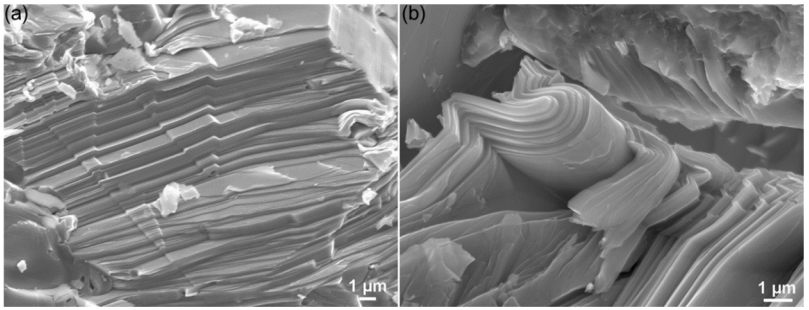

Fig. 1-2: SEM micrographs of the damage modes observed in the fracture surface of Cr_2AlSiC: (a–b) morphologies of kink bands[13].

Fig. 1-3 presents the potential applications for the MAX phases[15], including heating elements (a and b), gas burner nozzles in corrosive environments (c), high-temperature bearings (d), diamond/Ti_3SiC_2 composites for dry drilling of concrete (developed with Hilti Corp.) (e), examples of very thin walled parts manufactured by slip casting (f and g).

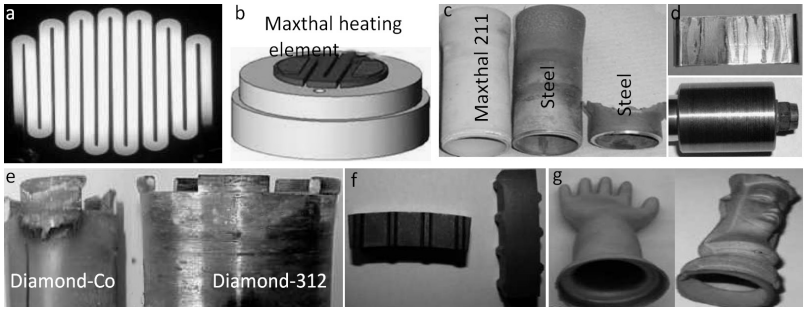

Fig. 1-3: Example of potential MAX phases applications courtesy of Kantal Corp. and 3-ONE-2[15].

1.1.2. Crystallographic structure and electronic structure of MAX phases

Crystallographic structure

The MAX phases are layered materials that crystallize in the hexagonal $P6_3/mmc$ space group. The unit cells of M_2AX, M_3AX_2 and M_4AX_3 phases are given in Fig. 1-4. One can notice that each structure consists of

alternate near-close-packed edge-sharing octahedral [M_6X] interleaved with layers of pure A elements. The main difference, among the structures of the so-called 211, 312 and 413 phases, is the number of M layers in between every two A layers. As can be seen in Fig. 1-4, two M layers exist in between two A layers in the 211 phases, and three M layers and four M layers in between two A layers in the 312 and 413 families, respectively.

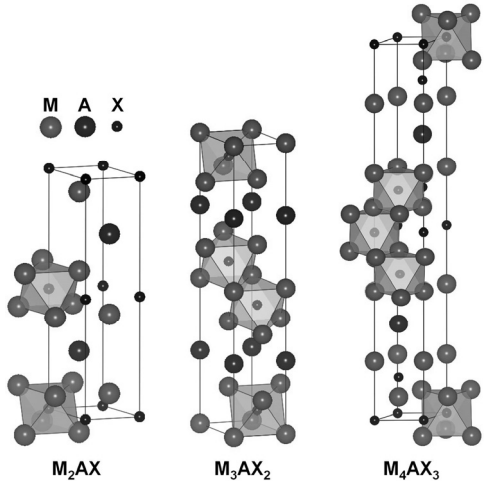

Fig. 1-4: The unit cells of the MAX phases for (a) 211, (b) 312 and (c) 413 classes.

Electronic structure of Ti_2AlC and Ti_2AlN

The electronic structure of a large number of MAX phases has been calculated (for 211 see [16-18], for 312 see [19-21] and for 413 see [22, 23]) through Density Functional Theory (DFT). In this section, we will focus on the electronic band structure, Total Density of States (TDOS) and Partial Density of States (PDOS) of one 413 phase (Ti_4AlN_3), one 312 phase (Ti_3SiC_2) and the two 211 phases investigated in this thesis (Ti_2AlC and Ti_2AlN). All of the reports indicate that there is no gap between the valence band and the conduction band. As a result, MAX phases should present metal-like conductivity, as indeed is demonstrated experimentally. At the Fermi level, the TDOS is mainly dominated by M 3d states, suggesting that the 3d states of the M element dominate the MAX phase's electronic conductivity. One can also notice that, for all MAX phases, the band structure shows strong anisotropic features. In Ti_3SiC_2, Ti_2AlN and Ti_2AlC, the bands are much less dispersive along the c-axis (i.e., along the Γ-A, H-K and M-L directions) than along the basal plane (i.e., along the Γ-

K and Γ-M directions). The Fermi velocity ($\partial E/\partial k$) should be higher along the basal plane than along the c-axis which would also result in very different conductivities in the basal plane and out of the basal plane. Finally, the strong ionic-covalent bonds between M and X and relatively weak ionic-covalent bonds between M and A formed in the (M_{II}-X-M_I-A) or (M_{II}-X-M_I-X-M_{II}-A) or (M_{II}-X-M_I-X-M_{II}-X-M_I-A) unit chains are responsible for the MAX phase high modulus and strength.

For example, the electronic band structure and the TDOS of Ti_2AlC and Ti_2AlN MAX phases, calculated by Hug et al. [24] in the frame of full-potential linearized augmented plane-waves formalism and tested using the generalized gradient approximation for the influence of the exchange and correlation potential, are shown respectively in Figs. 1-5 and 1-6. Minimization of the total energy with respect to the unit cell volume was adopted; the volume deviation was less than 1% between calculation and experiment. The electronic band structures are similar to the ones calculated by Zhou et al.[18]. In Fig. 1-5, it is clear that the bands are much less dispersive along the c-axis (i.e., along the Γ-A, H-K and M-L directions) than along the basal plane (i.e., along the Γ-K and Γ-M directions). This suggests that the electronic properties of Ti_2AlC and Ti_2AlN are anisotropic. The Fermi velocity ($\partial E/\partial k$) should be higher along the basal plane than along the c-axis.

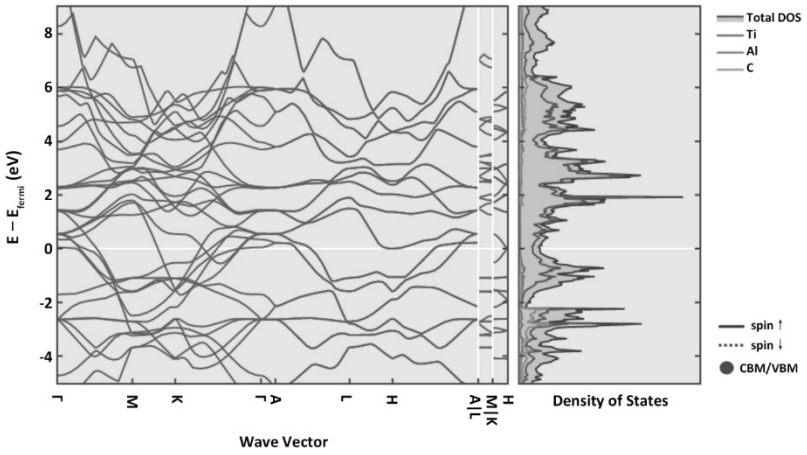

Fig. 1-5: The electronic band structure of Ti_2AlC MAX phases, TDOS and partial density of states of Ti_2AlC MAX phases.

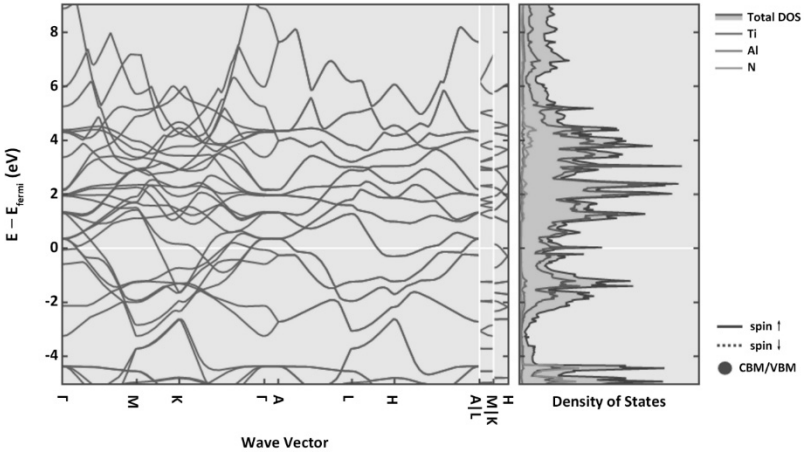

Fig. 1-6: The electronic band structure of Ti_2AlN MAX phases, TDOS and partial density of states of Ti_2AlN MAX phases.

Fig. 1-5 and Fig. 1-6 show the TDOS of the Ti_2AlC (a) and Ti_2AlN (b) MAX phases. Far from the Fermi level (E_F), the deep states are separated from the others by a gap of about 2 eV in the case of Ti_2AlC (-11.5 to -9.5 eV) and about 6.67 eV in the case of Ti_2AlN (-15.2 to -8.4 eV). The gap width is more or less important according to the composition of the MAX phase [24-26]. The bands continue from -8eV to the conduction band. There is no gap at the Fermi level which indicates that Ti_2AlC and Ti_2AlN have a metallic character as indeed has been demonstrated experimentally[27]. From the PDOS of Ti_2AlC and Ti_2AlN, one can notice that the PDOS of the two compounds is dominated, at the Fermi level, by the Ti-d states[24]. For Ti_2AlC and Ti_2AlN, the chemical bonding is dominated by strong hybridizations of Ti-d and Al-p states just below the Fermi level and of Ti p and N s (C s) states. The main difference in the electronic structure of these two compounds is related to the energy level of the hybridized states, such as Ti d –X p, X s. The N s (-15.9 to -15.1eV) and Ti d –N p (-6.7 to -4.2 eV) states are located at a lower energy level, compared to that of C s (-11.2 to -9.5 eV) and Ti d –C p (-5.2 to -2.1 eV) states. The gap difference has been attributed to the stronger electronegativity of N than C[24]. The charge transfers from the Al atom to Ti and N atoms in Ti_2AlN are much higher than the ones from the Al atom to Ti and C atoms in Ti_2AlC. As a result, stronger Ti-X bonds and Ti d-Al p bonds are expected in Ti_2AlN[24]. These calculations also predict that the electronic conductivity should be higher in Ti_2AlN than in Ti_2AlC, which is consistent with

experimental results[28].

Therefore, ionic-covalent Ti d-C/N p bonds are much stronger than ionic-covalent Ti d-Al p bonds. Thus, strong hybridization of Ti d-C/N p states is mainly responsible for the Ti_2AlC and Ti_2AlN high modulus and strength. The metal-like behavior of the Ti_2AlN and Ti_2AlC electronic transport properties results from the Ti d states.

1.2. MAX phase solid solutions

1.2.1. Substitution at M, A and X positions

It is worth noting that, in MAX phases, M, A and X elements either belong to the same group or are close to each other. As a consequence, the chemical and physical properties of the elements of each site are quite similar. One thus expects MAX phases to form a large number of isostructural solid solutions. In this section, some of the solid solutions reported in the literature will be described, as a function of the substitution site, in terms of synthesis techniques, microstructural characteristics and physical properties. As the MAX phase solid solutions synthesized in this manuscript are focused on substitution at the X site, an exhaustive discussion of the literature results will only be reported on these solid solutions.

Substitution at M site

Table 1-1 summarizes the synthesis conditions and some microstructural characteristics of different $(M_xM'_{1-x})_{n+1}AX_n$ solid solutions. $(Ti_{0.5}Zr_{0.5})_2InC$[29], $(Ti_{0.5}Nb_{0.5})_2AlC$[30], $(Ti_xV_{1-x})_2AlC$[31] and $(Cr_{0.5}V_{0.5})_2AlC$[32] can be synthesized by different techniques, such as Hot Isostatic Pressing (HIPing), and Hot Pressing (HPing), in the temperature range 1180-1600 °C. Most of the initial reactant mixtures contain the elements which constitute the final MAX phase solid solution (except for $(Ti_{0.5}Nb_{0.5})_2AlC$[30] which has been prepared from Al_4C_3). Some impurities such as MC binary carbides[29, 30], oxide of the A-element[30, 32] and MM' intermetallics[30] are detected in the final products.

In 2003, ab initio total energy calculations of the solubility of the M element within $(M_xM'_{2-x})AlC$ solid solutions (M and M'=Ti, V, Cr) have been performed by Sun et al.[33]. These results suggest that solubility is expected in the case of $(Cr_{1-x}V_x)_2AlC$ and $(Ti_{1-x}V_x)_2AlC$. Sun et al. have also predicted a strengthening effect (i.e., the bulk modulus is above the value given by a pure rule of mixture) in the $(M_xM'_{2-x})AlC$ (M and M' = Ti, V, Cr) system. These results have also been refined by Wang and Zhou

who have investigated the elastic stiffness and band structures of $(M_x,M'_{2-x})AlC$ solid solutions (M and M' = Ti, V, Cr) by means of the ab initio pseudo-potential total energy calculation method[34].

Table 1-1: Synthesis conditions and microstructural characteristics of some $(M_xM'_{1-x})_{n+1}AX_n$ solid solutions.

Process-ing methods	Nominal composi-tion	Synthesis conditions	Phase composition Lattice parameters (Å)	Micro-structure	Ref.
HIPing	Ti:Zr:In:C	PSing 650 °C/10 h/vacuum + HIP 1300 °C/12 h/70 MPa	$(Ti_{0.5}Zr_{0.5})_2InC$ (95 vol.%) TiC_x and ZrC_x (5 vol.%)	GS: 20-30 µm	[29]
	Ti:Nb:Al: C	1600 °C/8 h/100 MPa	$(Ti_{0.5}Nb_{0.5})_2AlC$ (98 vol.%) Al_2O_3 and Nb-Ti (2 vol.%) a=3.077 c=13.79	GS: 45 µm	[30]
	Ti:V:Al:C	1600 °C/8 h/70 MPa	$(Ti_{0.5}V_{0.5})_2AlC$ Al_2O_3 (2 vol.%)	GS: 25 µm	[35]
HPing	Ti:V:Al:C	1450 °C/1 h/20 MPa	$(Ti_xV_{1-x})_2AlC$ (x=0.05-0.2) Single phase *a* and *c* change linearly with x	GS: 39 µm in diameter and 19µm in thickness (all samples)	[31]
	Cr:V:Al: C	1180°C/8h/1.5GPa	$(Cr_{0.5}V_{0.5})_2AlC$ and $(Cr_{0.5}V_{0.5})C$ a=2.9773 c=12.0619	GS: 4-5µm	[32]
	Ti:Nb:Al: C	1450°C/24h/100 MPa	$(Ti_{0.5}Nb_{0.5})_2AlC$ Al_2O_3 and Nb-Ti (2 vol.%)	GS: 15µm Hv=5.8GPa	[30]

Substitution at the A-site

Table 1-2 lists the synthesis techniques and some microstructural characteristics of $M_{n+1}[A_{1-x}A'_x]C_n$ solid solutions. As is the case for $(M_xM'_{1-x})_{n+1}AX_n$ solid solutions, different techniques such as HIPing, HPing and Pressureless Sintering (PSing) have been used to synthesize $Ti_3(Al_xSn_{1-x})C_2$[34, 36], $Ti_3(Al_xSi_{1-x})C_2$[37, 38], $Ti_3(Si_xGe_{1-x})C_2$[39, 40], $Cr_2(Al_{0.96}Si_{0.13})C$[41] and $Cr_2(Al_xGe_{1-x})C$[42] in the temperature range 1200 - 1600 °C. Some impurities such as MC binary carbides[39, 40], oxide of the A-element[41] and MA intermetallics[41] were detected in the final products.

Wang et al.[43] and Xu et al.[44] predicted, through a plan-wave pseudo-potential method based on DFT, that lattice parameters of $Ti_3(Si_{1-x}Al_x)C_2$ would follow Vegard's law with increasing Al content. This result was partially proven by Zhou et al.[37] by investigating $Ti_3(Si_{1-x}Al_x)C_2$ ($x \leq 0.25$) solid solutions. Indeed, the *c*-lattice parameter decreases with increasing Si content whereas the *a*-lattice parameter remains almost unchanged. Recently, a set of $Ti_3(Al_xSn_{1-x})C_2$ solid solutions has been successfully synthesized by Dubois et al.[34, 36] through HIPing process at the PPRIME Institute. It has been demonstrated that $Ti_3(Al_xSn_{1-x})C_2$ are ideal solid solutions obeying Vegard's law since the c/a ratio varies linearly with the Al content. Furthermore, it has been shown that solid solution strengthening is not operative in the Ti-Al-Sn-C system. Elastic modulus is found to increase non-monotonically from Ti_3SnC_2 to Ti_3AlC_2[34]. Similar results (i.e., no solid solution strengthening) have been obtained by Ganguly et al.[39] for the $Ti_3(Si_{(1-x)}Ge_x)C_2$ solid solutions.

Table 1-2: Synthesis conditions and microstructural characteristics of some $M_{n+1}[A_{1-x}A'_x]C_n$ solid solutions (GS: grain size).

Process-ing methods	Nominal compositi on	Synthesis conditions	Phase composition Lattice parameters (Å)	Micro-structure	Ref.
HIPing	Ti:Sn:Al: C Ti:Sn:Al: C	1200-1500 °C/1-8 h/50 MPa	$Ti_3(Al_xSn_{1-x})C_2$ (Main phase) TiC and $Ti_2(Al_xSn_{1-x})C$ *c/a* changes linearly with x	GS:10-80 µm Solid solution softening	[34, 36]
	3Ti:0.5G e:0.5Si:2 C	1450 °C/8 h/172 MPa	$Ti_3(Si_{0.5}Ge_{0.5})C_2$ (96vol.%) TiC (4 vol.%) a=3.082 c=17.751	GS: 7 ±3 µm	[39, 40]
	3Ti:0.25 Ge:0.75S i:2C	1600 °C/8 h/172 MPa	$Ti_3(Si_{0.75}Ge_{0.25})C_2$ (97vol.%) TiC (3 vol.%) a=3.074 c=17.747	GS: 70±56 µm	[39, 40]
HPing	Ti:(1-x)Al:xSi: C (x≤0.25)	1500 °C/1 h/30 MPa	$Ti_3(Al_{1-x}Si_x)C_2$ single phase a is stable *c* changes linearly with x	GS: 20 µm	[37, 38]
	2Cr:1.1A l:0.2Si:C	1450 °C/1 h/30 MPa	$Cr_2(Al_{0.96}Si_{0.13})C$ Minor impurities: Al_2O_3 and Cr_5Si_3	GS: 50 µm	[41]
PSing	Cr:Al:Ge: C	1400°C/4h/ Ar	$Cr_2(Al_xGe_{1-x})C$ (x=0,0.25,0.5,0.7 5,1) *c*-lattice parameter increases with x *a*-lattice parameter decreases with x	Not mention-ed	[42]

Substitutions at X site

Table 1-3 summarizes the synthesis conditions and some microstructural characteristics of $Ti_{n+1}Al(C_xN_{1-x})_n$ solid solutions. As compared to the studies dedicated to solid solutions on the M and A sites, only two elements (C and N) correspond to the X site in MAX phases. Only HIPing and PSing have been used to synthesize $Ti_3Al(C_{0.5}N_{0.5})_2$[45, 46], $Ti_2Al(C_{0.5}N_{0.5})$[45, 47] and $Ti_2Al(C_xN_{(1-x)})_y$ (x = 0; 0.25; 0.5; 0.75; 1 and 0.7 ≤ y ≤1)[48] in the temperature range 1300-1400 °C. Some impurities such as TiC[45, 46], Ti(C,N)[6], Al_2O_3[45, 47], TiAl[48] intermetallics and the Ti_3AlC_2[48] MAX phase were detected in the final products. It thus appears as a challenge to synthesize highly pure $Ti_2Al(C_xN_y)$ phases.

As MAX carbonitrides, $Ti_2Al(C_xN_{1-x})$ phases are one of the most important examples of MAX phase solid solutions on the X site. Since Ti-N and Ti-C have similar chemical bonding characteristics, resembling those of binaries TiC and TiN compounds[49], it is thus possible to form a wide range of $Ti_2Al(C_xN_{1-x})$ solid solutions with different physical properties. For example, a $Ti_2Al(C_{0.5}N_{0.5})$ solid solution is reported to be significantly harder than either of its end-members Ti_2AlC and Ti_2AlN. Stoichiometric and substoichiometric $Ti_2Al(C_xN_{(1-x)})_y$ solid solutions have been recently synthesized by Cabioc'h et al.[48] with x = 0; 0.25; 0.5; 0.75; 1 and 0.7≤ y ≤1 by reactive PSing for 4 h at 1400 °C. The authors have shown that irrespective of the number of vacancies on the X site, the *a*-lattice parameter obeys Vegard's law whereas the *c*-lattice parameter of the carbonitrides is smaller than that of the end-members.

Table 1-3: Synthesis conditions and microstructural characteristics of some $Ti_{n+1}Al(C_xN_{1-x})_n$ solid solutions (GS: grain size).

Process-ing methods	Nominal composi-tion	Synthesis conditions	Phase composition Lattice parameter(Å)	Micro-structure	Ref.
HIPing	Ti:Al:C:N	1400 °C/10 h/100 MPa	$Ti_3Al(C_{0.5}N_{0.5})_2$ (95vol.%) TiC (2 vol.%) Al_2O_3 (3 vol.%) c/a changes linearly with C content	GS: 25±15 μm	[45, 46]
	Ti:Al:0.5 C:0.5N	1300 °C/15 h/40 MPa	$Ti_2Al(C_{0.5}N_{0.5})$ (96 vol.%) Al_2O_3 and Ti_3P (4 vol.%)	GS: 25 μm Solid solution strengthening	[45, 47]
PSing	Ti:1.1Al: C:N	1400 °C/4 h/ Ar	$(Ti_2AlC_xN_{1-x})_y$ With minor impurities: Ti_3AlC_2,TiAl, Ti(C,N)	GS: 2-10 μm	[48]

In 1999, Barsoum et al. reported[45, 47, 50] the solid solution strengthening effect in the Ti-Al-C-N system using microindentation tests. For the two Ti_2AlC and Ti_2AlN end-members, their hardness values were about 4.5 GPa and 4 GPa, respectively. The $Ti_2AlC_{0.5}N_{0.5}$ solid solution sample had a value of around 5.5 GPa.

In 2007, Radovic[45] reported Poisson's ratio, Young's modulus E, shear modulus G and longitudinal v_l and shear v_s sound velocities of $Ti_2AlC_{0.5}N_{0.5}$ and two Ti_2AlN samples[51, 52] (more details about their microstructural characteristics are given in Table 1-2). The different parameters measured for $Ti_2AlC_{0.5}N_{0.5}$ and for both end-members [45, 51, 53] by Resonant Ultrasound Spectroscopy (RUS)[45] are listed in Table 1-4. It was found that substituting C with N increased E and G in the solid solution. Furthermore, the decrease in v_s for $Ti_{1.93}AlN_{0.975}$ as compared to $Ti_2AlN_{0.996}$ was attributed to the influence of vacancies; this phenomenon was also reported in binary TiX compounds[54]. For example, ab initio

calculations predict that the introduction of 12.5% vacancies in TiN_x reduces its shear modulus from 180 GPa to less than 150 GPa[55], which is in compatible agreement with experimental results[4].

Table 1-4[45]: Summary of Young's modulus E, shear modulus G, longitudinal v_l and shear v_s sound velocities measured by RUS.

Sample	Composition	E (GPa)	G (GPa)	v_l (m/s)	v_s (m/s)	Reference
Ti_2AlC	Not measured	278	119	8590	5423	[53]
$Ti_2AlC_{0.5}N_{0.5}$	Not measured	290	123	8670	5407	[45]
Ti_2AlN(a)	$Ti_2AlN_{0.996}$	285	120.5	8553	5328	[45, 51]
Ti_2AlN(b)	$Ti_{1.93}AlN_{0.975}$	277	112	8700	5100	[45, 51]

1.3. Physical properties of MAX phases

1.3.1 Hardness measured by microindentation and nanoindentation tests

Table 1-5 summarizes hardness values of selected MAX phases determined either by microindentation or by nanoindentation tests.

The Vicker's hardness values of polycrystalline MAX phases were distributed in the 3-8 GPa range for microindentation tests, which is much lower than the ones obtained by nanoindentation tests (which were in the range 7-12 GPa). Such a difference has been studied by Bei et al. [34]. As an example, Bei et al. measured Ti_3AlC_2 hardness using nanoindentation and microindentation tests; the results are given in Fig. 1-7. Using the nanoindentation test, Ti_3AlC_2 hardness is a function of the indenter penetration depth, which is attributed to an indentation size effect. Such an effect is well fitted by the Nix and Gao model[56] and hardness reaches a limiting value of 11.4±0.7 GPa[34] for penetration depths in the range 200-300 nm. Such a limiting value is defined as the intrinsic hardness of Ti_3AlC_2. For deeper penetration depth (in the range 400-600 nm in Fig. 1-7), nanoindentation and microindentation tests lead to the same hardness

values (about 7 GPa in Fig. 1-7). At deeper penetration depths (in the range 600-1700 nm in Fig. 1-7), hardness values measured by microindentation tests continue to decrease. Considering MAX phase grain size, in the range of 2-100 µm[41, 47, 57, 58] several grains are involved in the deformation process during microindentation or nanoindentation tests performed at large indenter penetration depths [34]. Thus, hardness values determined at high loads (large penetration depths) consist of a mean value that takes into account grain boundaries and also impurities (TiC[59, 60], TiN[6] and oxide TiO_2[61], Al_2O_3[30, 57]). Upon increasing the penetration depth, more and more grain boundaries and impurities have to be taken into account and thus this leads to a decrease of the microindentation hardness values. Finally, one can extract the intrinsic hardness of MAX phases through nanoindentation in order to avoid the influence of second phases, impurities and grain boundaries. Moreover, a local determination of the MAX phase composition and grain size may allow determining the stoichiometry and grain sizes effects on mechanical properties (elastic modulus and hardness).

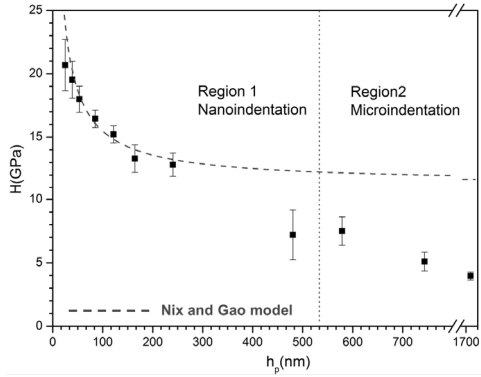

Fig. 1-7[34]: Hardness (squares) of Ti_3AlC_2 as a function of the indenter penetration depth in nanoindentation tests and microindentation tests.

Ti_2AlC hardness values, determined using microindentation tests, were in the range 2.8-5.8 GPa. Such differences in the values may result from grain size and/or carbon stoichiometry. Indeed, Bai et al. have determined, using microindentation tests, that 6 µm grained $Ti_2AlC_{0.69}$ has a hardness value of 5.8 GPa[62]. Yu et al.[41] have measured, using microindentation tests, hardness values of coarse-grained (CG) and fine-grained (FG) Cr_2AlC. A large grain size effect has been evidenced (see Table 1-5). Nevertheless, the reliability of the results is not good considering what has

Table 1-5: Summary of hardness and Young's modulus of selected MAX phases determined by microindentation and nanoindentation tests (L: length of lamella, W: width of lamella). The grain size values are given as average diameters.

	Sample	Grain size (μm)	Phase composition	Load	Hardness (GPa)	Young's modulus (GPa)	Reference
Microindentation	$(Ti_x,V_{1-x})_2AlC$ (x=0.2)	W:19 ± 5 L:39 ± 10	$(Ti_{0.8}V_{0.2})_2AlC$	10 N	3.5-4.5		[31]
	Ti_2AlN	100	10-20 vol.% Al_2O_3, Ti_3P and Ti_4AlN_3	0.5-10 N	4	285	[47]
	$Ti_2AlC_{0.5}N_{0.5}$	25	4 vol.% Al_2O_3 and Ti_3P	0.5-10 N	5.5	290	[47]
	Ti_2AlC	W: 5 L: 20	pure	10N	2.8		[63]
	Ti_2AlC	25	10-15 vol.% Al_2O_3 and Ti_3P	0.5-10 N	4.5		[47]
	Ti_2AlC	W:16 ± 4 L:41 ± 12	Ti_2AlC	10 N	3.5		[31]
	$Ti_2AlC_{0.69}$	6	$Ti_2AlC_{0.69}$ TiAl	50 N	5.8		[62]
	Ti_2AlC	15	pure	10 N	4.2-5.7		[58]
	Cr_2AlC	35	pure	500 N	3.5		[41, 57]
	Cr_2AlC	2	pure	500 N	6.4		
	Ti_2SC	2-4	6 vol.% TiO_2	2-300 N	7-8		[61]
		10-20			6-7		
	Ti_3AlC_2	5	pure	100 N	5.5-6		[60]
	Ti_3AlC_2	35	pure	100 N	3.5-4.5		

Nanoindentation	Ti_3AlC_2	W: 10-40 L: 60-100	pure	1-250 mN	11.4±0.7	260	[34] [64]
	$Ti_3Al_xSn_{(1-x)}C_2$ X=0.25,0.5,0.8		$Ti_3Al_xSn_{(1-x)}C_2$ $Ti_2Al_xSn_{(1-x)}C$ TiC	1-300 mN	7-11	200-250	[36] [34]
	Ti_3SnC_2	W: 3-5 L: 10-15	80.5%Ti_3SnC_2 16.2% TiC 1.1% $FeSn_x$ 2.2% Sn	1-300 mN	9.3	245	[65]